

Simultaneous construction of dual Borgen plots. I: The case of noise-free data

Mathias Sawall^a, Annekathrin Jürß^a, Henning Schröder^{a,b}, Klaus Neymeyr^{a,b}

^aUniversität Rostock, Institut für Mathematik, Ulmenstrasse 69, 18057 Rostock, Germany

^bLeibniz-Institut für Katalyse, Albert-Einstein-Strasse 29a, 18059 Rostock

Abstract

In 1985 Borgen and Kowalski [DOI:10.1016/S0003-2670(00)84361-5] introduced a geometric construction algorithm for the regions of feasible nonnegative factorizations of spectral data matrices for three-component systems. The resulting Borgen plots represent the so-called Area of Feasible Solutions (AFS). The AFS can be computed either for the spectral factor or for the factor of the concentration profiles. In the latter case, the construction algorithm is applied to the transposed spectral data matrix. The AFS is a low-dimensional representation of all possible nonnegative solutions, either of the possible spectra or of the possible concentration profiles.

This work presents an improved algorithm for the simultaneous construction of the two dual Borgen plots for the spectra and for the concentration profiles. The new algorithm makes it possible to compute the two Borgen plots roughly at the costs of a single classical Borgen plot. The new algorithm comes without any loss of precision or spatial resolution. The new method is benchmarked against various program codes for the geometric-constructive and for the numerical optimization-based AFS computation.

Key words: multivariate curve resolution, Borgen plot, nonnegative matrix factorization, area of feasible solutions, polygon inflation, *FACPACK*.

1. Introduction

In model-free multivariate curve resolution (MCR) the aim is to extrapolate from the spectral observation of a chemical reaction system to the contributions from the underlying pure components. If a series of spectra is measured and if these spectra are written as the rows of a k -by- n spectra matrix D , then the Lambert-Beer law

$$D = CS^T + E \quad (1)$$

expresses an approximate bilinear relation between D and the nonnegative factors $C \in \mathbb{R}^{k \times s}$ and $S \in \mathbb{R}^{n \times s}$. The error term E is assumed to be small or to vanish. The columns of C are the concentration profiles of the s pure components and the columns of S are the associated pure component spectra [15, 14]. If only D is given, then the computation of chemically interpretable factors C and S is a difficult problem as (1) with $E = 0$ can have many nonnegative solutions. This fact is known under the keyword *rotational ambiguity*, see e.g. [34, 2]. Additional information on the reaction system can help to reduce this ambiguity. Here we pursue the approach to

compute the complete range of all nonnegative factorizations $D = CS^T$ and to represent the possible factors columnwise in the low-dimensional form of the *Area of Feasible Solutions* (AFS). Such AFS analyses are well-known for two-, three- and four-component systems. These techniques can be classified as either geometric constructive approaches [13, 16, 5, 23, 11] or as numerical optimization-based approaches [1, 7, 27, 8, 31]. In recent years many new methods or modifications of established methods have been devised; see the review works [6, 26]. Some of these methods have reduced the computational costs for determining the AFS considerably. The computation times are about seconds for medium-sized data sets and are up to minutes for multi-megabyte data sets.

1.1. Motivation and aim of the paper

Against the background of an increasing importance of model-free MCR methods, which are always faced with the problem of the non-uniqueness of their results due to the so-called rotational ambiguity, we present a new, very efficient algorithm which simultaneously constructs the AFS sets for the concentration factor and

for the spectral factor. This new algorithm is based on a geometric construction in terms of Borgen plots [16, 5, 23, 22, 11, 12]. It does not include any numerical approximations. Therefore the algorithm provides precise results - however, small rounding errors are unavoidable if the algorithm is implemented on a computer. As is typical for Borgen plots, the algorithm can only be applied to non-perturbed and noise-free model data. This disadvantage will be compensated in a forthcoming second part of this paper, where the algorithm is extended in a way that it can be applied to perturbed, noisy experimental spectral data. This extended algorithm is of a hybrid nature, as it combines the geometric construction with the numerical approximation underlying the polygon inflation algorithm [27, 28]. The new methods work accurately and are very fast.

In this first part, we analyze a certain duality of the polygons INNPOL and FIRPOL, see Sec. 3 and [10, 21]. This duality can be used in a way that a facet of INNPOL for the one factor makes it possible to construct a vertex of FIRPOL for the other factor. Such a duality is already known in the community. What is new is that the duality is exploited in order to build a fast and precise construction of the AFS for the concentration factor and *simultaneously* for the spectral factor. For each constructed boundary point of the AFS of one factor the new method forms two inner boundary points of the AFS for the other factor. Our analysis is partially general in a sense that it applies to any dimension. Then INNPOL and FIRPOL are polyhedra. The forthcoming second part of the paper combines the speed and precision of the geometric construction with the robustness for perturbed and noisy data of optimization-based methods. Such a robustness is the benefit of the numerical AFS computation methods as polygon inflation, triangle enclosure or grid-search. The new algorithm simultaneously computes the two AFS sets almost as fast as the classical Borgen plot algorithm computes a single AFS for ideal model data.

1.2. Organization of the paper

The paper is organized as follows: Sec. 2 introduces the SVD-based approach to the MCR problem and to the AFS. Sec. 3 defines certain important sets and polyhedra for the subsequent geometric constructions, contains their analysis and presents an indirect and very fast computation method, which is based on the complementarity/duality theory. The central new results on the simultaneous geometric construction of the AFS sets for noise-free data are presented in Sec. 4. Finally, the results are compared to the results of other methods (polygon inflation and generalized Borgen plots) in Sec. 5.

1.3. Notation

The following notation is used in the paper.

D	$k \times n$ spectral data matrix by Eqs. (1), (2).
C	$k \times s$ concentration matrix by Eq. (1).
S	$n \times s$ spectra matrix by Eq. (1).
$U\Sigma V^T$	singular value decomposition of D by Eq. (2).
T	$s \times s$ transformation matrix by Eqs. (2), (3).
\mathcal{M}	AFS spectral factor by Eq. (4).
\mathcal{M}_C	AFS concentration factor by Eq. (5).
\mathcal{I}	INNPOL spectral factor by Eq. (8).
\mathcal{I}_C	INNPOL concentration factor by Eq. (9).
\mathcal{F}	FIRPOL spectral factor by Eq. (8).
\mathcal{F}_C	FIRPOL concentration factor by Eq. (9).
a_i	scaled left singular vectors by Eq. (6).
b_j	scaled right singular vectors by Eq. (7).

2. MCR and the AFS

A well-established approach to the construction of nonnegative factors $C \in \mathbb{R}^{k \times s}$ and $S \in \mathbb{R}^{n \times s}$ for a given rank- s matrix $D \in \mathbb{R}^{k \times n}$ is to use a singular value decomposition (SVD) $D = U\Sigma V^T$ of D , see [9]. Here we consider a truncated SVD in a way that U and V have only s columns and that Σ is an s -by- s diagonal matrix with the s dominant singular values of D on its diagonal. Then the product $U\Sigma V^T$ is the best rank- s approximation of D in the least-squares sense [9, 33]. The truncated SVD is important in the case of perturbed data with $E \neq 0$ in (1) so that $D \approx U\Sigma V^T$. For ease of presentation we consider $E = 0$ in the sequel. The key idea for the construction of C and S is to insert a transformation $T \in \mathbb{R}^{s \times s}$ and its inverse in the truncated SVD in a way that

$$D = U\Sigma V^T = \underbrace{U\Sigma T^{-1}}_{=C \geq 0} \underbrace{TV^T}_{=S^T \geq 0}. \quad (2)$$

Only those T are considered for which C and S are nonnegative matrices. A purely numerical approach is to determine the matrix elements of T by solving an optimization problem, see e.g. [35, 19].

2.1. Sets of feasible spectra and concentration profiles

If (2) holds for a certain T and P is a permutation matrix, then this equation holds also for PT instead of T (then T^{-1} is substituted by $T^{-1}P^T$). This operation rearranges the columns of C and S in the same way. Consequently the set of all possible first columns of S is equal to the set of all possible columns of S (i.e. the

possible spectra). We denote this set by \mathcal{S} and the corresponding set of possible concentration profiles by \mathcal{C} so that

$$\begin{aligned}\mathcal{C} &= \{u \in \mathbb{R}^k : (2) \text{ holds with } C(:, 1) = u\}, \\ \mathcal{S} &= \{v \in \mathbb{R}^n : (2) \text{ holds with } S(:, 1) = v\}.\end{aligned}$$

If an algorithm is available which allows us to determine the set \mathcal{S} , then \mathcal{C} can be formed by applying this algorithm to $D^T = SC^T$ as C and S have changed their places by transposition. We call a spectrum v feasible if matrices $C, S \geq 0$ exist so that v equals the first column of S and $D = CS^T$.

2.2. The AFS

The set \mathcal{S} is unbounded as any positive multiple ωv for $v \in \mathcal{S}$ and $\omega > 0$ is consistent with (2) if the associated u is substituted by u/ω . The unboundedness can easily be avoided by fixing a certain scaling. Therefore each matrix element in the first column of T is set equal to 1

$$T = \begin{pmatrix} 1 & x_1 & \cdots & x_{s-1} \\ 1 & & & \\ \vdots & & W & \\ 1 & & & \end{pmatrix}. \quad (3)$$

The justification that each vector in \mathcal{S} has a non-vanishing contribution from the first right singular vector relies on the Perron-Frobenius theory of nonnegative matrices [17], see [28] for the proof. This allows us to define the AFS as the set of the $(s-1)$ -dimensional row vectors

$$\begin{aligned}\mathcal{M} &:= \{x \in \mathbb{R}^{s-1} : \text{exists } W \in \mathbb{R}^{(s-1) \times (s-1)} \text{ with} \\ &T(1, 2 : s) = x^T, \text{rank}(T) = s \text{ and } C, S \geq 0\} \quad (4)\end{aligned}$$

with T and W by (3); see [7, 27, 26]. Some basic properties of the AFS, not only that \mathcal{M} is bounded and does not include the origin, are proved in [28, 11, 31]. These proofs require the (mild) assumptions that DD^T and $D^T D$ are irreducible matrices.

The corresponding AFS for the factor C is defined as

$$\begin{aligned}\mathcal{M}_C &= \{y \in \mathbb{R}^{s-1} : \text{exists } T \in \mathbb{R}^{s \times s}, \text{rank}(T) = s, \\ &(T^{-1})(:, 1) = \begin{pmatrix} 1 \\ y \end{pmatrix} \text{ and } U\Sigma T^{-1} \geq 0, TV^T \geq 0\}. \quad (5)\end{aligned}$$

2.3. AFS computations

For two-component systems ($s = 2$) the AFS can explicitly be written in dependence on the matrix elements of D , see [13, 2, 28, 26, 31]. For three- and four-component systems various and differing AFS computation methods are available. As already mentioned in

Sec. 1, the algorithms for three-component systems are either of geometric-constructive nature [5, 23, 11] or are based on the solution of numerical optimization problems [2, 7, 27, 31]. For four-component systems the pioneering work has been done in [8, 6, 26, 31].

The focus of this work is on three-component systems. A new technique is developed which determines the (boundaries of the) sets \mathcal{M} and \mathcal{M}_C simultaneously. The details of this new method are explained in Sec. 4. In the next, preparatory section we define and analyze two important supersets of \mathcal{M} and \mathcal{M}_C .

3. Fast computation of FIRPOL

This section deals with the polygons FIRPOL and INNPOL as introduced by Borgen and Kowalski [5] and, e.g., later used in [23, 11]. Here the representation is not restricted to polygons ($s = 3$) but applies to polyhedra of arbitrary dimensions $s \geq 3$. The construction of the polyhedra FIRPOL and INNPOL is the first step for the geometric construction of the spectral AFS \mathcal{M} and its pendant \mathcal{M}_C for the concentration factor. In the following we describe and analyze various duality relations between the polyhedra FIRPOL and INNPOL for each \mathcal{M} and \mathcal{M}_C . These results relate facets of INNPOL with vertices of FIRPOL. Finally, we describe an approach how the polyhedra FIRPOL (both for the spectral factor and for the concentration factor) can be computed in a fast indirect way.

The underlying duality relations are known, see Henry [10] and Rajkó [21]. The duality has been used in [3] for the effective construction of the polygons FIRPOL and INNPOL for the two factors. The decisive point of the duality analysis in this section is to show that extremal points of INNPOL are one-to-one related to halfplanes which include facets of the dual polygon FIRPOL. Similarly, inner points of INNPOL are also one-to-one related to dual halfplanes which do not contribute to the boundary of FIRPOL.

The duality is also expressed in some complementarity theory, see, e.g., [24, 30, 18]. However, a simultaneous construction algorithm for Borgen plots, in which a single triangle rotation process is used in order to construct the two AFS sets by using duality relations, has not been described or published.

3.1. A remark on the duality principle

In general, duality in mathematics is a principle which refers to two (mathematical) objects which stand in a one-to-one relation. Properties of one of these objects can often be translated to related properties of the

second object. Duality relations are well known in optimization theory, mathematical logic, set theory and many other fields. In this paper, the term duality refers to various properties of the representing sets of two factors C and S^T of D and their construction.

3.2. Data representation and affine hyperplanes

In order to construct the boundaries of \mathcal{M} and \mathcal{M}_C some auxiliary objects are required. The starting point is the SVD $D = U\Sigma V^T$ which can be written in the equivalent forms

$$DV = U\Sigma \quad \text{and} \quad \Sigma^{-1}U^TD = V^T.$$

The first equation can be interpreted in a way that it represents the expansion coefficients of the i th row of D with respect to the basis of right singular vectors by the i th row of $U\Sigma$. The second equation is the corresponding or *dual* representation of the columns of D with respect to the basis of scaled (with the singular values) left singular vectors; the columns of V^T contain the expansion coefficients. These vectors of expansion coefficients together with the normalization as used in (3)–(5) are the $(s-1)$ -dimensional column vectors

$$a_i := \frac{((U\Sigma)(i, 2:s))^T}{(U\Sigma)(i, 1)} = \frac{(U\Sigma)^T(2:s, i)}{U^T(1, i)\sigma_1} \quad (6)$$

for $i = 1, \dots, k$ and the column vectors

$$b_j := \frac{V^T(2:s, j)}{V^T(1, j)} \quad (7)$$

for $j = 1, \dots, n$.

Borgen and Kowalski [5] in their geometric construction of \mathcal{M} for the case $s = 3$ defined the polygons \mathcal{F} (called FIRPOL) and \mathcal{I} (called INNPOL) by means of the a_i and b_j . For general $s \geq 3$, these polyhedra have the form

$$\begin{aligned} \mathcal{F} &= \{x \in \mathbb{R}^{s-1} : V \begin{pmatrix} 1 \\ x \end{pmatrix} \geq 0\}, \\ \mathcal{I} &= \text{convhull}\{a_i : i = 1, \dots, k\}, \end{aligned} \quad (8)$$

see also [23, 11]. The definition of the analogous sets for the concentration factor C read

$$\begin{aligned} \mathcal{F}_C &= \{y \in \mathbb{R}^{s-1} : U\Sigma \begin{pmatrix} 1 \\ y \end{pmatrix} \geq 0\}, \\ \mathcal{I}_C &= \text{convhull}\{b_j : j = 1, \dots, n\}. \end{aligned} \quad (9)$$

These latter sets are required for the construction of \mathcal{M}_C .

The superset FIRPOL, denoted by \mathcal{F} , of \mathcal{M} is by its definition the intersection of the n affine half-spaces which are given by the n components of the inequality $V(1, x^T)^T \geq 0$. These n affine half-spaces are one-sided bounded by the n affine hyperplanes (which derive from the j th component of $V(1, x^T)^T = 0$)

$$E_j^{(S)} := \left\{ x \in \mathbb{R}^{s-1} : \frac{V(j, 2:s)x}{V(j, 1)} = -1 \right\} \quad (10)$$

for $j = 1, \dots, n$. Analogously, the affine hyperplanes

$$E_i^{(C)} = \left\{ y \in \mathbb{R}^{s-1} : \frac{U\Sigma(i, 2:s)y}{U(i, 1)\sigma_1} = -1 \right\}, \quad (11)$$

for $i = 1, \dots, k$ belong to the affine half-spaces $U\Sigma(1, y^T)^T \geq 0$. Each of these affine half-spaces is oriented in a way that it contains the origin. The intersection of these spaces is the superset \mathcal{F}_C of \mathcal{M}_C .

3.3. Duality of points and affine hyperplanes

Next relations from \mathcal{I}_C to \mathcal{F} are analyzed. Analogous relations hold for \mathcal{I} and \mathcal{F}_C . These relations and their analysis are the basis of the construction algorithms for \mathcal{F} and \mathcal{F}_C . The starting point for the analysis is the complementarity and coupling theory in [24]. This theory is closely related to the duality principles as stated by Henry [10] and Rajkó [21]. The duality describes mathematical constraints for the columns of C if certain columns of S are known and vice versa. The constraints are given in the form of (affine) linear equations for the unknown parts. Typically, the theory provides major restrictions, i.e. small subsets of the AFS can be identified which include the feasible solutions. For a discussion and for the analysis of the constraining conditions, see [21, 4, 30]. For example, a central result is that a fixed point in the AFS \mathcal{M} (i.e. a certain pure component spectrum is known) restricts the representations of the remaining components in the concentrational AFS \mathcal{M}_C to an affine hyperplane. In short, a point in one AFS set is dual (or complementary) to an affine hyperplane in the other AFS set and vice versa.

Definition 3.1. A vector $z \in \mathbb{R}^{s-1}$ and an affine hyperplane $E = \{y \in \mathbb{R}^{s-1} : y^T z_E = -1\}$ are called dual (or complementary) if $z_E = z$.

An elementary consequence of Def. 3.1 is the following corollary.

Corollary 3.2. According to Def. 3.1 the a_i by (6) and the hyperplanes $E_i^{(C)}$ by (11) are dual for $i = 1, \dots, k$. In the same way, the b_j by (7) and the hyperplanes $E_j^{(S)}$ are dual for $j = 1, \dots, n$.

In words Cor. 3.2 is about the duality of a_i , whose convex hull equals \mathcal{I} , and the hyperplanes $E_i^{(C)}$ which underlie the construction of \mathcal{F}_C . The next lemma describes a similar relation of points on the boundary of \mathcal{F}_C to dual hyperplanes which are tangential to \mathcal{I} , cf. Sec. 3 in [21]. Fig. 1 illustrates the relations.

Lemma 3.3. *The point $y_0 \in \mathbb{R}^{s-1}$ is a boundary point of \mathcal{F}_C if and only if the dual affine hyperplane E to y_0 is a tangential plane to \mathcal{I} (which does not intersect the interior of \mathcal{I}) and at least one index $i_0 \in \{1, \dots, k\}$ exists so that a_{i_0} by (6) is a point of tangency of E to \mathcal{I} .*

Proof. First $y_0 \in \mathcal{F}_C$, that means $U\Sigma \begin{pmatrix} 1 \\ y_0 \end{pmatrix} \geq 0$, is equivalent to

$$(U\Sigma)(:, 2 : s)y_0 \geq -U(:, 1)\sigma_1.$$

Equivalently it holds for all $i \in \{1, \dots, k\}$ that

$$\frac{(U\Sigma)(i, 2 : s)y_0}{U(i, 1)\sigma_1} \geq -1 \quad (12)$$

or $a_i^T y_0 \geq -1$ with a_i by (6). Equality in (12) for one index i_0 , i.e. $a_{i_0}^T y_0 = -1$, is equivalent to y_0 being located on the boundary of \mathcal{F}_C .

The dual affine hyperplane to y_0 reads by its definition $E = \{x \in \mathbb{R}^{s-1} : x^T y_0 = -1\}$. Hence (12) shows that all a_i are located in the half-spaces on one side of the affine hyperplane E . The convex hull of the a_i equals \mathcal{I} so that E cannot intersect the interior of \mathcal{I} . Finally, $a_{i_0} \in E$ is a point of tangency since $a_{i_0}^T y_0 = -1$ as shown above. This proves the two directions of the if-and-only-if conditional statement. \square

Lemma 3.3 can be reformulated for points on the boundary of \mathcal{F} which are set in relation to tangential affine hyperplanes of \mathcal{I}_C , see Fig. 1.

Corollary 3.4. *Let $x_0 \in \mathbb{R}^{s-1}$ be located on the boundary of \mathcal{F} . Then the dual affine hyperplane E to x_0 is a tangential plane to \mathcal{I}_C . At least one index $j_0 \in \{1, \dots, n\}$ exists so that b_{j_0} by (7) is a point of tangency of E to \mathcal{I}_C . This point satisfies*

$$V(j_0, 2 : s)x_0 = -V(j_0, 1)$$

or equivalently $b_{j_0}^T x_0 = 0$.

The next step is to extend Lemma 3.3 in a way that the vertices of \mathcal{F}_C are shown to be the dual points of the affine hyperplanes which include facets of the polyhedron \mathcal{I} . Up to now we have proved that the tangential hyperplanes touch the polygon at least in a vertex. It remains to show that this hyperplane contains an edge (for $s = 3$) or in general a facet of \mathcal{I} . This is the basis for computing the vertices of \mathcal{F}_C by using the polyhedron \mathcal{I} and also to compute the vertices of \mathcal{F} by using \mathcal{I}_C .

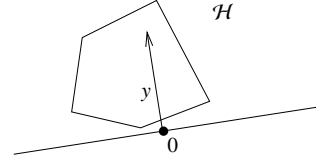


Figure 3: A convex set which does not include the origin is necessarily a subset of a half-plane \mathcal{H} defined by an appropriate $y \neq 0$.

3.4. Duality of the facets of \mathcal{I} and the vertices of \mathcal{F}_C

This section analyzes a duality of the facets of \mathcal{I} and the vertices of \mathcal{F}_C . First we show that the origin is an interior point of \mathcal{I} .

Lemma 3.5. *Let DD^T be an irreducible matrix. Then the origin $x = 0$ is an interior point of \mathcal{I} .*

Proof. We assume $x = 0$ not to be an interior point of \mathcal{I} . Then the convexity of \mathcal{I} implies that \mathcal{I} is a subset of the half-plane

$$\mathcal{H} = \{z \in \mathbb{R}^{s-1} : z^T y \geq 0\}$$

for a proper nonzero vector $y \in \mathbb{R}^{s-1}$, see Fig. 3. Further (6) implies that

$$0 \leq a_i^T y = \frac{1}{\sigma_1 U(i, 1)} U\Sigma(i, 2 : s)y, \quad i = 1, \dots, k,$$

which reads in vectorial form

$$\frac{1}{\sigma_1} \text{diag}(1/U(1, 1), \dots, 1/U(k, 1)) U\Sigma(:, 2 : s)y \geq 0.$$

Since $\sigma_1 > 0$ and as the first singular vector $U(:, 1)$ can be assumed strictly positive (due to the Perron-Frobenius theory on the assumption of irreducibility of DD^T), the last equation proves that $U\Sigma(:, 2 : s)y \geq 0$ for the given $y \neq 0$. This contradicts Corollary 2.3 in [28] for irreducible DD^T since a nonnegative and nonzero linear combination of the columns of $U\Sigma$ always has a nonzero contribution from the first singular vector $U(:, 1)$. \square

The Lemma 3.3 is needed in order to prove that the vertices of \mathcal{F}_C and the facets of the polyhedron \mathcal{I} are dual. Facets are nondegenerate faces of a polyhedron, i.e. the dimension of a facet is one less the dimension of the polyhedron (or mathematically a facet has the codimension 1). See Fig. 2 of an illustration of the content of the following theorem.

Theorem 3.6. *Let $D^T D$ and DD^T be irreducible matrices with D of the rank $s \geq 3$. A point y_0 is a vertex of \mathcal{F}_C if and only if its dual affine hyperplane E contains a facet of \mathcal{I} , i.e. a face of the codimension 1.*

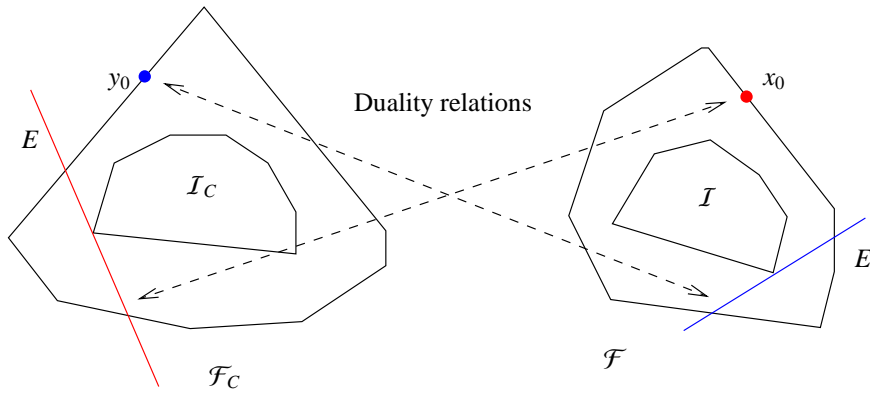


Figure 1: Lemma 3.3 describes a duality relation of a boundary point $y_0 \in \mathcal{F}_C$ to a tangential plane of \mathcal{I} as well as of a boundary point $x_0 \in \mathcal{F}$ to a tangential plane of \mathcal{I}_C .

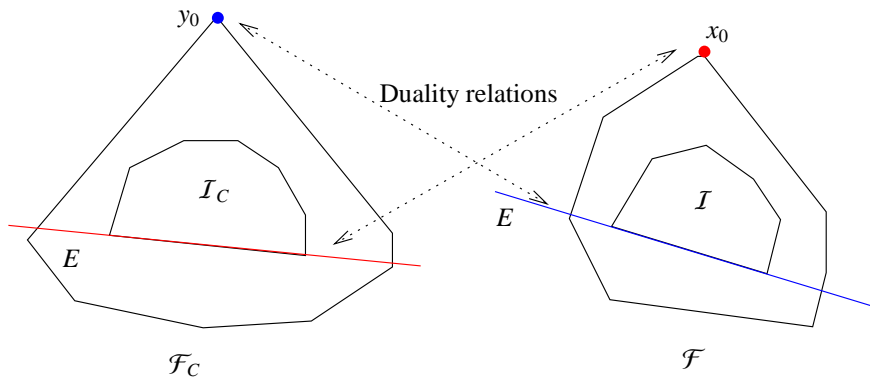


Figure 2: Theorem 3.6 describes a duality relation of a vertex $y_0 \in \mathcal{F}_C$ to a tangential plane of \mathcal{I} which encloses a facet of \mathcal{I} . Further a vertex $x_0 \in \mathcal{F}$ is dual to a tangential plane of \mathcal{I}_C which contains a facet of \mathcal{I} .

Proof. First we prove the direction that a facet of \mathcal{I} is dual to a vertex y_0 of \mathcal{F}_C . In order to show that a dual vector y_0 in the sense of Def. 3.1 exists, we have to prove that the facet is enclosed by an affine hyperplane and not only by a hyperplane. (The crucial point is that Def. 3.1 with $y^T z_E = -1$ specifies an affine hyperplane which does not include the origin.) Due to Lemma 3.5 the origin $\mathbf{0} = (0, \dots, 0)^T \in \mathbb{R}^{s-1}$ is an interior point of \mathcal{I} . Hence the facet E of \mathcal{I} cannot contain the origin. Thus a dual vector y_0 exists which represents the affine hyperplane E in the form $E = \{x \in \mathbb{R}^{s-1} : y_0^T x = -1\}$. It remains to show that y_0 is a vertex of \mathcal{F}_C .

As E contains a facet (codimension 1) of \mathcal{I} , there exist $s-1$ affine independent vertices $a_{i_1}, \dots, a_{i_{s-1}}$ by (6) whose convex hull equals the facet. Therefore it holds that

$$y_0^T a_{i_j} = -1, \quad j = 1, \dots, s-1, \quad (13)$$

$$y_0^T a_\ell \geq -1, \quad \ell \in \{1, \dots, k\} \setminus \{i_1, \dots, i_{s-1}\}. \quad (14)$$

Thus (13) and (14) show that y_0 fulfills the condition $U\Sigma(1, y_0)^T \geq 0$ for a membership in \mathcal{F}_C according to (9). Furthermore from (13) it follows that y_0 belongs to exactly $s-1$ of the affine hyperplanes which enclose \mathcal{F}_C . For the selected indexes i_1, \dots, i_{s-1} these $s-1$ affine hyperplanes are linearly independent. Hence y_0 is a vertex of \mathcal{F}_C (and not only an interior point of an edge). This completes the proof of the first direction.

In order to prove the other direction let y_0 be a vertex of \mathcal{F}_C . As y_0 is a vertex it holds that in $s-1$ components of $U\Sigma(1, y_0^T)^T \geq 0$ equality is attained. Let i_1, \dots, i_{s-1} be the indexes of these components. Reversing the arguments of the first part of the proof proves that the dual hyperplane E encloses the facet of \mathcal{I} with the vertices $a_{i_1}, \dots, a_{i_{s-1}}$. \square

Analogously, this result is valid for facets of \mathcal{I}_C and the dual vertices of \mathcal{F} , see Fig. 2.

Corollary 3.7. *On the assumptions of Thm. 3.6 the following equivalence holds: A point x_0 is a vertex of \mathcal{F} if and only if its complementary affine hyperplane E contains a facet of \mathcal{I}_C .*

The duality results of Thm. 3.6 enable a fast computation of \mathcal{F}_C if the polyhedron \mathcal{I} is known, see the following Sec. 3.5. Additionally, the duality helps to determine the sets \mathcal{F} and \mathcal{I} even in the presence of noise or perturbations, see the second part of this paper.

Fig. 4 illustrates the duality of the facets of \mathcal{I} to the vertices of \mathcal{F}_C as well as the duality of the facets of \mathcal{I}_C to the vertices of \mathcal{F} . These figures have been generated for a three-component model problem which is taken

from the *FACPACK*-homepage, see [29] for the details. Related pairs of objects (vertices and edges of the polygons) are marked by the same, continuously changing color. Additionally, Fig. 5 illustrates these relations for a four-component model problem. Vertices of the three-dimensional polyhedrons are dual to the 2D-facets of the dual polyhedra.

3.5. Fast computation of \mathcal{F} and \mathcal{F}_C

The sets \mathcal{F} and \mathcal{I} are decisive ingredients for the geometric construction of \mathcal{M} , see [16, 5, 23, 11, 12]. The same geometric construction algorithm applied to \mathcal{F}_C and \mathcal{I}_C leads to the AFS \mathcal{M}_C for the concentration factor. The sets \mathcal{F} and \mathcal{F}_C are intersections of the n , respectively k , affine hyperplanes (10) and (11) which are oriented each in a way that they include the origin. Our approach for the fast computation of the four polyhedra \mathcal{F} , \mathcal{I} , \mathcal{F}_C and \mathcal{I}_C can significantly decrease the computation times for \mathcal{M} and \mathcal{M}_C .

This section introduces a direct and also an indirect approach for the computations of \mathcal{F} and \mathcal{F}_C . These approaches are based on Thm. 3.6 and Cor. 3.7. A comparison of these techniques for a three-component model problem is contained in Sec. 5.2. The following two subsections focus on \mathcal{F} ; everything can easily be reformulated for \mathcal{F}_C .

3.5.1. Direct computation of \mathcal{F}

A direct and intuitive approach to compute the polyhedron \mathcal{F} is as follows: Initially s affine half-spaces are selected in a way that their intersection is bounded. Then all other affine half-spaces (which finally tightly enclose \mathcal{F}) are analyzed whether or not a further reduction of the current intersection can be gained. If so, then the new smaller intersection is the new approximation to \mathcal{F} . This iteration terminates in \mathcal{F} . See also the approach in [23].

3.5.2. Indirect computation of \mathcal{F}

The polyhedron \mathcal{F} can also be computed in an indirect way as already suggested by Beyramysoltan et al. [3], see Sec. 3. The formal mathematical justification (which requires the irreducibility of the matrices $D^T D$ and DD^T) is given in Thm. 3.6 and Cor. 3.7. Following [3], first \mathcal{I}_C is computed by simply forming the convex hull of the vectors b_j , see Eq. (9). `MATLAB` provides for this the routine `convhull`. In a second step for each facet of \mathcal{I}_C its dual vertex of \mathcal{F} is computed.

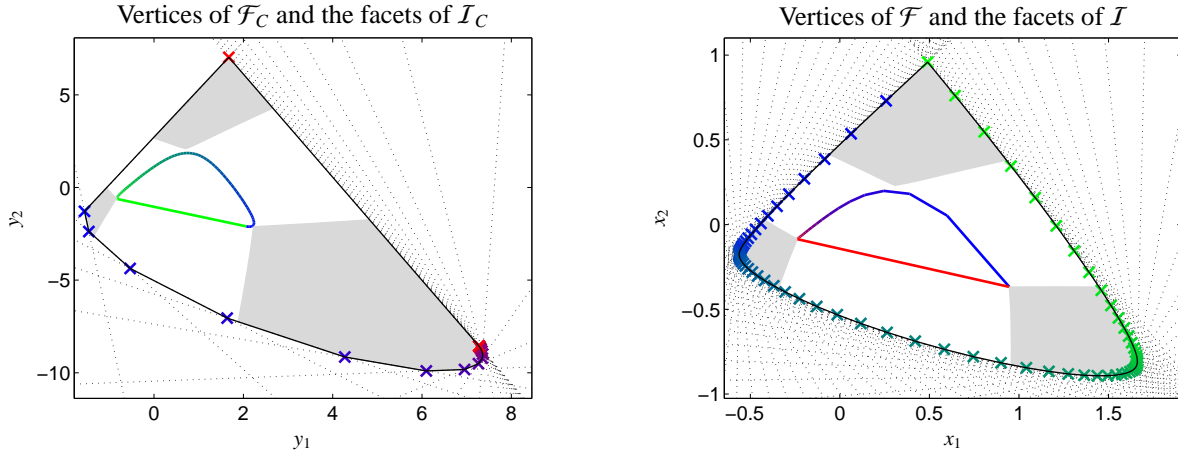


Figure 4: The duality of the facets of I and the vertices of \mathcal{F}_C and also the duality of the facets of I_C and the vertices of \mathcal{F} is illustrated for the three-component model problem from [29]. Left: The sets I_C, \mathcal{F}_C as well as the three isolated subsets of the AFS \mathcal{M}_C (in gray) are shown. Right: The sets I, \mathcal{F} as well as the three isolated subsets of the AFS \mathcal{M} (in gray) are shown. The series of dotted lines encloses and defines the convex set \mathcal{F}_C (left) respectively \mathcal{F} (right); the boundaries of these two sets are drawn by black solid lines. The dual pairs of facets of I_C and vertices of \mathcal{F} are each plotted by using the same color. Analogously, the same colors are used for the dual pairs of facets of I and vertices of \mathcal{F}_C .

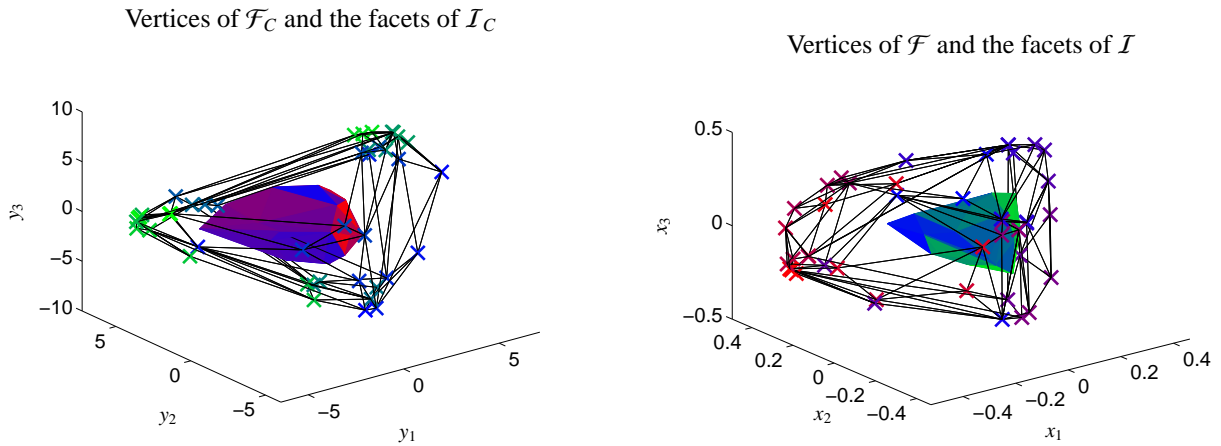


Figure 5: The duality of the facets of I and the vertices of \mathcal{F}_C and also the duality of the facets of I_C and the vertices of \mathcal{F} are illustrated for a four-component model problem. Left: The sets I_C and \mathcal{F}_C are shown. Right: The sets I and \mathcal{F} are drawn. The edges of the polyhedra \mathcal{F}_C and \mathcal{F} are plotted by black lines. The dual pairs of facets of I_C and vertices of \mathcal{F} are plotted by using the same color. Analogously, the same colors are used for dual pairs of facets of I and vertices of \mathcal{F}_C .

4. Simultaneous computation of \mathcal{M} and \mathcal{M}_C for three-component systems

In 1985 Borgen and Kowalski [5] introduced the geometric construction of the AFS for three-component systems ($s = 3$) on the basis of results gained in [13, 16]. The method was revitalized by Rajkó [23] in 2005 and has been extended in [11, 12]. The idea of the geometric construction is to form the inner boundary of \mathcal{M} by means of all triangles which enclose INNPOL and which are enclosed by FIRPOL (\mathcal{F}). In combination with the polygon \mathcal{F} , which is a superset of the AFS \mathcal{M} , this yields the boundary of the AFS. This boundary comprises of separate closed curves if the AFS consists of isolated subsets. We call these subsets the *segments* of the AFS.

In contrast to the numerical AFS approximation by means of solving optimization problems, the benefit of a geometric construction of the AFS is that the inner boundary points of the AFS can be constructed exactly. However, the boundary of the AFS is in general not a polygon, but consists of a sequence of smooth curves which are joined to a continuous boundary curve. The construction of the smooth boundary curves requires a discretization of the problem and results in approximation errors and also in the unavoidable small rounding errors by the computer arithmetic. The computational costs for the geometric construction are relatively low. Furthermore, degenerated segments of the AFS, namely points or line segments, can also be computed precisely (aside from the small numerical rounding errors). Borgen plots are ideal tools for the investigation of theoretical questions on noise-free and non-perturbed model data. For experimental noisy data some modifications of the Borgen plot construction are required. In [11, 12] an extended construction algorithm has been presented which can deal with small perturbations. Nevertheless, the purely numerical methods in [2, 7, 27] are still more robust for AFS computations for experimental spectral data.

This section presents a new method for the simultaneous geometric construction of the spectral AFS and also the AFS for the concentration factor. The new construction algorithm can form the two AFS sets at costs which are slightly higher than the costs for constructing only one AFS set by the classical algorithm. This is a considerable improvement on the classical approach with double costs if the two AFS sets \mathcal{M} and \mathcal{M}_C are constructed in separate steps.

In this section we first define *inner boundary points* and prove a certain property of these points. The classical Borgen plot construction is briefly reviewed and

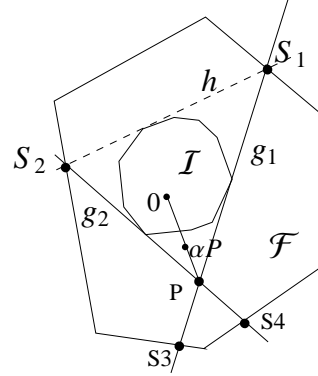


Figure 6: Construction of inner boundary points by triangles tightly including \mathcal{I} with the vertices S_1 and S_2 on the boundary of \mathcal{F} and a third vertex in \mathcal{F} .

the new simultaneous construction is explained. The suggested method is tested for a model problem whose AFS consists of an isolated point, a line segment and a bounded planar segment.

4.1. Inner boundary points

The following definition of an inner boundary point refers to the ray casting concept for AFS computations as suggested in [31]. The definition is not limited to the case $s = 3$.

Definition 4.1. A point $x \in \mathcal{M}$ is called an inner boundary point if $\gamma x \notin \mathcal{M}$ for all $\gamma \in (0, 1)$. In words x is the only member of \mathcal{M} on the line segment from the origin 0 to x . A point $x \in \mathcal{M}$ is called an outer boundary point if $\gamma x \notin \mathcal{M}$ for all $\gamma > 1$.

A direct consequence of these definitions is summarized in the next remark.

Remark 4.2. A point $x \in \mathcal{M}$ can belong to the inner and to the outer boundary according to Def. 4.1. Special examples are punctiform or line-shaped AFS segments.

The key idea of the geometric construction of the AFS for three-component systems [16, 5, 23, 11] is that the inner boundary points are constructed by certain triangles. Each of these triangles is a triangle which tightly includes \mathcal{I} , is contained in \mathcal{F} and has two of its vertices on the boundary of \mathcal{F} . Then the third vertex is an inner boundary point. This property is proved in the next lemma.

Lemma 4.3. For $s = 3$ let h be a tangent of \mathcal{I} . The two points of intersection of h with the boundary of \mathcal{F} are S_1 and S_2 , see Fig. 6. Let g_1 be a further tangent of \mathcal{I} which runs through S_1 and g_2 be another tangent of \mathcal{I} which

runs through S_2 so that h , g_1 and g_2 tightly enclose \mathcal{I} . The point of intersection of g_1 and g_2 is denoted by P .

If $P \in \mathcal{F}$, then P is an inner boundary point of \mathcal{M} .

Proof. We consider the case that $P \in \mathcal{F}$. Then the triangle construction guarantees that $P \in \mathcal{M}$, see [5]. We assume P not to be an inner boundary point of \mathcal{M} and derive a contradiction. If P is not an inner boundary point, then an α with $0 < \alpha < 1$ exists so that αP is closer to the origin and is still an element of \mathcal{M} , see Fig. 6. As αP is a feasible point, two other points S' and S'' exist in \mathcal{F} so that the triangle Δ' with the vertices αP , S' and S'' includes \mathcal{I} and is contained in \mathcal{F} . The geometry in the AFS plane, see Fig. 6, shows (by considering tangents of \mathcal{I} which run through αP) that P , S' and S'' are on the same side of h . Moreover, S' and S'' are not located on h as \mathcal{I} is a convex set with a positive volume (since the origin is an interior point of \mathcal{I}). Thus the line segment S' -to- S'' which is an edge of Δ' must intersect \mathcal{I} . This is a contradiction to Δ' including \mathcal{I} . \square

4.2. Classical Borgen plots

The tangent-rotation method for the geometric construction of the AFS for three-component systems is explained, e.g., in [5, 23, 11, 12]. The basic idea is to rotate a tangent h around the polygon \mathcal{I} . For each tangent an inner boundary point P is constructed in the way as explained in Lemma 4.3. In a computer implementation the rotation of the tangent is discretized by considering only a fixed number of equiangular tangents. In order to find all critical boundary points, one also considers all tangents which coincide with a facet of \mathcal{I} and also the families of possible tangent lines at vertices of \mathcal{I} . In order to detect line-shaped (1D) AFS segments additional tangents are to be analyzed. This process results in a finite set of points which discretizes the boundary curve of the inner boundary. The outer boundary of \mathcal{M} coincides with a subset of the boundary of \mathcal{F} . The spatial resolution of the inner boundary increases with a decreasing finite rotation angle of the tangent. In the generalized Borgen plot module of *FACPACK* [29] we typically use 3600 equiangular tangents in order to attain a sufficiently resolved boundary of \mathcal{M} .

4.3. Simultaneous Borgen plots

The standard approach to compute the Borgen plot for the concentration factor is to apply the algorithm to the transposed data matrix D^T . This doubles the costs for the construction of \mathcal{M} and \mathcal{M}_C compared to a construction of only \mathcal{M} . The simultaneous construction of the dual Borgen plots determines the inner boundary of

\mathcal{M}_C as a by-product of the construction of the spectral AFS \mathcal{M} . In contrast to the classical Borgen plots each tangent h is not only used to construct a single triangle, but three of them. In terms of the notation used in Lemma 4.3 these two additional triangles result in the two points Q and R which are possible candidates for inner boundary points of \mathcal{M}_C .

4.3.1. Construction of the inner boundary of \mathcal{M}_C

We continue with the notation from the proof of Lemma 4.3, see Fig. 6. Let Δ be the triangle with the vertices P , S_1 and S_2 . Furthermore, let S_3 be the second point intersection of g_1 with the boundary of \mathcal{F} in a way that $S_3 \neq S_1$. Based on this construction the dual point of the line through S_2 and S_3 is an inner boundary point of \mathcal{M}_C provided that this point is located in \mathcal{F}_C . This is proved next in Thm. 4.4. Furthermore it is possible to compute a second auxiliary triangle with the vertices S_1 , S_2 and S_4 where S_4 is the second point of intersection of g_2 and the boundary of \mathcal{F} with $S_4 \neq S_2$. Then the dual point of the line through S_1 and S_4 is an inner boundary point of \mathcal{M}_C provided that the point is located in \mathcal{F}_C .

Theorem 4.4. *Let the three points Q_1 , Q_2 and Q_3 be located on the boundary of \mathcal{F} and span the triangle Δ , see Fig. 7. The triangle Δ is assumed to include \mathcal{I} . Let the two edges through Q_1 be tangential to \mathcal{I} . Further, let Δ_1 be the triangle which is spanned by the dual points of the edges of Δ in the sense of Lem. 3.3. (Equivalently the three edges of Δ_1 are dual to either Q_1 , Q_2 or Q_3 .)*

Then the triangle Δ_1 fulfills the conditions of Lemma 4.3 and the point P which is dual to the line through Q_2 and Q_3 is an inner boundary point of \mathcal{M}_C provided that P is contained in \mathcal{F}_C .

Proof. Cor. 3.4 guarantees that the three straight lines which are dual to Q_1 , Q_2 and Q_3 are tangential to \mathcal{I}_C . These lines form a triangle Δ_1 (as Δ defines a feasible nonnegative factorization $D = CS^T$ with Δ_1 being related to C). See Fig. 7 for the geometry. Two of the edges of Δ are tangential to \mathcal{I} . Hence Lemma 3.3 proves that two vertices of Δ_1 are located on the boundary of \mathcal{F}_C . Thus Lemma 4.3 applies to the triangle Δ_1 with the vertices S_1 , S_2 and P and proves that P is an inner boundary point of \mathcal{M}_C provided that $P \in \mathcal{F}_C$. This point P is the dual point of the straight line through Q_2 and Q_3 , see the green line and point in Fig. 7. \square

Theorem 4.4 is the basis for the simultaneous Borgen plot algorithm which is explained next.

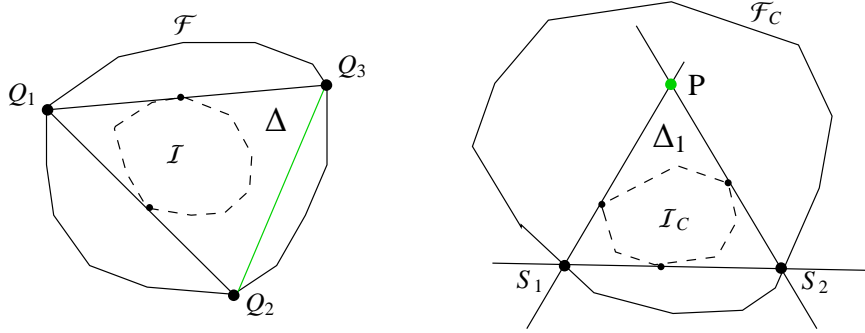


Figure 7: Simultaneous construction of points P on the inner boundary of M_C , see Thm. 4.4.

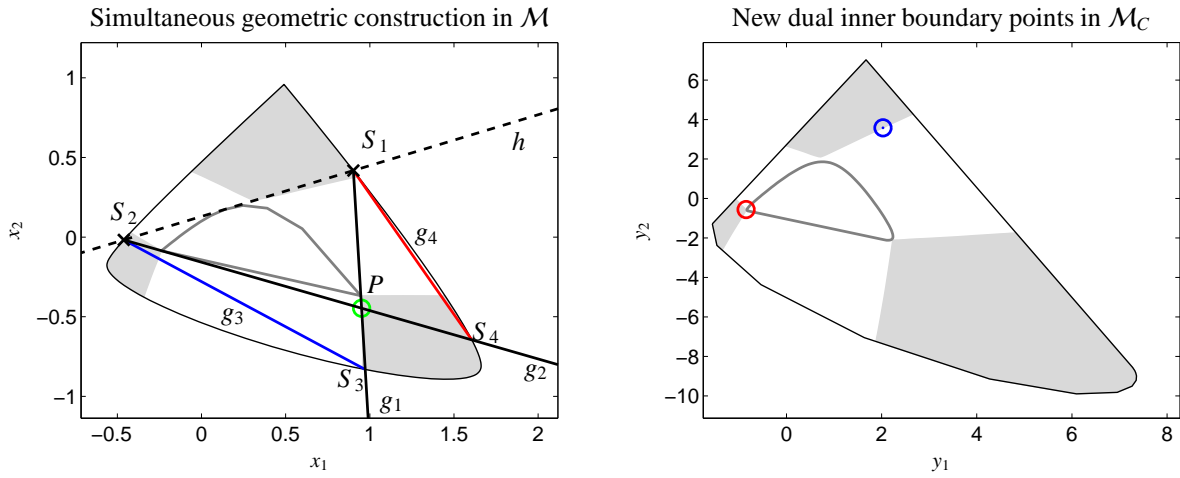


Figure 8: Demonstration of the extension of the classical Borgen plots in order to compute simultaneously an inner boundary point of M and two inner boundary points of M_C for the three-component model problem. Left: Geometric construction of an inner boundary point. For the tangent h (broken black line) the points of intersection S_1 and S_2 (\times) with the boundary of \mathcal{F} as well as the tangents g_1 and g_2 (black solid lines) to I are constructed. The point of intersection of g_1 and g_2 is the inner boundary point P (\circ). The points S_3 and S_4 are the points of intersection of g_1 respectively g_2 with the boundary of \mathcal{F} . The triangles with the vertices S_1, S_2 and S_3 respectively S_1, S_2 and S_4 fulfill the condition of Thm. 4.4. The dual point of g_3 (blue line) is contained in the dual plane which contains \mathcal{F}_C and is an inner boundary point of M_C (\circ in the right subplot). Also the dual point of g_4 (red line) belongs to \mathcal{F}_C and so it is an inner boundary point of M_C (\circ in the right plot). The resulting AFS sets M and M_C are plotted as gray areas. The boundaries of the supersets \mathcal{F} and \mathcal{F}_C are the black closed curves. The boundaries of the inner polygons I and I_C are plotted gray.

4.3.2. The algorithm

The construction of the inner boundary points of the AFS \mathcal{M}_C is embedded into the classical Borgen plot construction of the inner boundary points of the AFS \mathcal{M} . The only step which is basically different from the classical Borgen construction is that the computed inner boundary points of \mathcal{M}_C require a specific ordering. To this end we use polar coordinates.

The construction of the two inner boundary points of \mathcal{M}_C is based on Theorem 4.4. Only those points which belong to the superset \mathcal{F}_C successfully pass the construction. The starting point is a tangent h of \mathcal{I} .

1. The two points of intersection S_1 and S_2 of the tangent h of \mathcal{I} with the boundary of \mathcal{F} are constructed.
2. A first tangent g_1 of \mathcal{I} through S_1 with $g_1 \neq h$ and a second tangent g_2 of \mathcal{I} through S_2 with $g_2 \neq h$ are constructed.
3. The intersection of g_1 and g_2 is P . According to Lemma 4.3 P is an inner boundary point as far as $P \in \mathcal{F}$.
4. Additionally, the point of intersection S_3 of g_1 with the boundary of \mathcal{F} is determined (in a way that $S_3 \neq S_1$) and also the point of intersection S_4 of g_2 with the boundary of \mathcal{F} is computed (so that $S_4 \neq S_2$).
5. Then g_3 is the straight line through S_2 and S_3 . Further, g_4 is the straight line through S_1 and S_4 . According to Theorem 4.4 the dual point of g_3 is an inner boundary point of \mathcal{M}_C if it is contained in \mathcal{F}_C . Also the dual point of g_4 is an inner boundary point of \mathcal{M}_C if it is in \mathcal{F}_C .

Remark 4.5. *The point which is dual to g_3 is contained in the superset \mathcal{F}_C (and so it is an inner boundary point of \mathcal{M}_C) if and only if P is contained in \mathcal{F} (so that P is an inner boundary point of \mathcal{M}). An analogous statement holds for the point which is dual to g_4 .*

The complete algorithm is based on the rotation of the tangent h around \mathcal{I} . Practically, only a fixed number of m equiangular tangent lines are considered together with certain additional points which serve to detect punctiform or line-shaped AFS segments. At the end all constructed boundary points of the AFS \mathcal{M}_C are ordered with respect to their polar coordinates. This approach is justified by the gap-free intersection property of the AFS sets [31]; this property says that the intersection of an AFS with an infinite ray starting at the origin is either empty or a line-segment (which may be degenerated to a single point).

4.3.3. Visualization of the geometric construction

Fig. 8 illustrates the simultaneous Borgen plots for a three-component model problem. For a fixed tangent h of \mathcal{I} shows the construction of one inner boundary point of \mathcal{M} and two inner boundary points of \mathcal{M}_C . First the triangle of the classical Borgen plot yields an inner boundary point P . Then two additional triangles with the vertices S_1, S_2 and S_3 respectively S_1, S_2 and S_4 are formed. Finally, the dual points of g_3 respectively g_4 are plotted in the AFS \mathcal{M}_C for factor C . These two points are inner boundary points of \mathcal{M}_C (if located in \mathcal{F}_C).

Further, Fig. 9 shows the results of the simultaneous Borgen plot algorithm. The sequences of points on the inner boundaries of \mathcal{M} and \mathcal{M}_C are presented for a (relatively small) number of $m = 500$ tangents to \mathcal{I} . However, $m = 500$ leads to a sufficient spatial resolution for a graphical demonstration of the principles of simultaneous Borgen plots. The spatial resolution of the boundary of \mathcal{M}_C is twice as high as for \mathcal{M} since two boundary points of \mathcal{M}_C correspond to one boundary point of \mathcal{M} .

4.4. Detection of line segments and isolated points

An AFS can have various shapes. The AFS can either be a topologically connected set with a hole around the origin or can consist of several isolated subsets (the segments). For three-component systems ($s = 3$) the number of segments can be 1 or a multiple of 3. If \mathcal{M} consists of three or more segments, then one segment can equal an isolated point or it can be a one-dimensional line segment. Such degenerated segments can be observed for properly designed model data. The (simultaneous) Borgen plot algorithm can detect such degenerated AFS segments.

Next we demonstrate for

$$D = \begin{pmatrix} 1 & 1 & 1 \\ 0 & 1 & 1 \\ 0 & 0 & 1 \end{pmatrix} \quad (15)$$

that the simultaneous Borgen plot algorithm can find punctiform and line-shaped AFS segments as parts of \mathcal{M}_C , see the upper row of plots in Fig. 10. There is no necessity to demonstrate that these degenerated segments can correctly be detected in the spectral AFS \mathcal{M} as the simultaneous Borgen plot algorithm for the first AFS coincides with the classical Borgen plot construction from [5, 23, 11]; classical Borgen plots are well-known to construct degenerated AFS segments correctly.

The lower two subplots of Fig. 10 explain the triangle and point selection. The red and the green triangle (broken lines) are related to the line-shaped segment

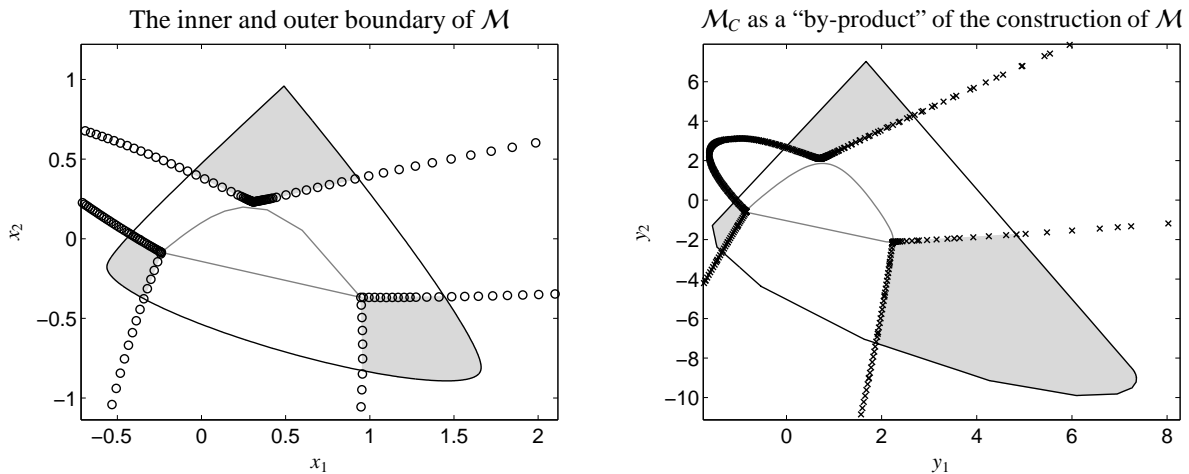


Figure 9: Simultaneous construction of M and M_C by the algorithm from Sec. 4.3.2. A number of $m = 500$ equiangular tangents h has been used for the computation of the inner boundary points of M . The steps 4 and 5 of the algorithm supply the by-product of the inner boundary points of M_C . Left: The combination of the (outer) boundary of \mathcal{F} (closed black curve) and the results for the inner boundary points (\circ) of M leads to the three isolated subsets of M (in gray). Right: The inner boundary (\times) of M_C is a by-product of the geometric construction for M . Together with boundary \mathcal{F}_C (closed black curve) this makes it possible to compute the three isolated subsets of the AFS M_C for the concentration factor (gray areas).

and also two critical points of the 2D-area segment of the AFS M . These two triangles are important for the classical Borgen plots. All vertices of these two triangles are located on the boundary of \mathcal{F} and all their edges are tangents of \mathcal{I} . Hence each edge of the two triangles yields a dual inner boundary point of M_C , see Thm. 4.4. These dual points are plotted in the lower right subplot. All points are significant (but two of them coincide) for the construction of the segments of M_C . The last point (in cyan), which is significant for the construction of the inner boundary of M_C , is the dual point of the cyan triangle (broken line) in the lower left plot. This triangle is part of the combined geometric construction. All other points on the inner boundary of M_C , which arise from the other tangents, do not influence the final result. Hence the simultaneous geometric construction leads to M_C as a by-product of the computation of M even for this problem with degenerated punctiform and line-shaped AFS segments.

5. Numerical results and computation times

This section demonstrates the effectiveness of simultaneous Borgen plots for a three-component model problem, see Sec. 5.1. We consider various discretizations of the model problem with increasing matrix dimensions. The underlying pure component spectra, the concentration profiles and the kinetic equations are always the same. The focus of the comparative analysis is on the computation times. These times are com-

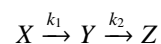
pared with some well-established methods. Simultaneous Borgen plots have at least the same precision (spatial resolution) as the classical geometric constructive Borgen plots.

We start with the construction and computation of \mathcal{F} and \mathcal{I} and their counterparts \mathcal{I}_C and \mathcal{F}_C . We compare the proposed indirect computation of \mathcal{F} , see Sec. 3, with the direct approach and also with the numerical approximation by means of the polygon inflation method. Then the simultaneous Borgen plot construction is compared with two separate runs of the classical Borgen plot construction. Finally, simultaneous Borgen plots are compared with the *FACPACK* implementations of the *polygon inflation method* [27, 28] and with the *generalized Borgen plots* [11, 12].

We run all computations on a single core of a 3.40GHz Intel CPU of a standard personal computer with 16GB RAM. The major part of the program is written in C; however some *MATLAB* routines, e.g. the routine *convhull*, have been used.

5.1. The three-component model problem

We consider the first-order consecutive reaction scheme



with $k_1 = 0.5$ and $k_2 = 0.1$ and the initial concentrations $c_X(0) = 1$ and $c_Y(0) = c_Z(0) = 0$. The

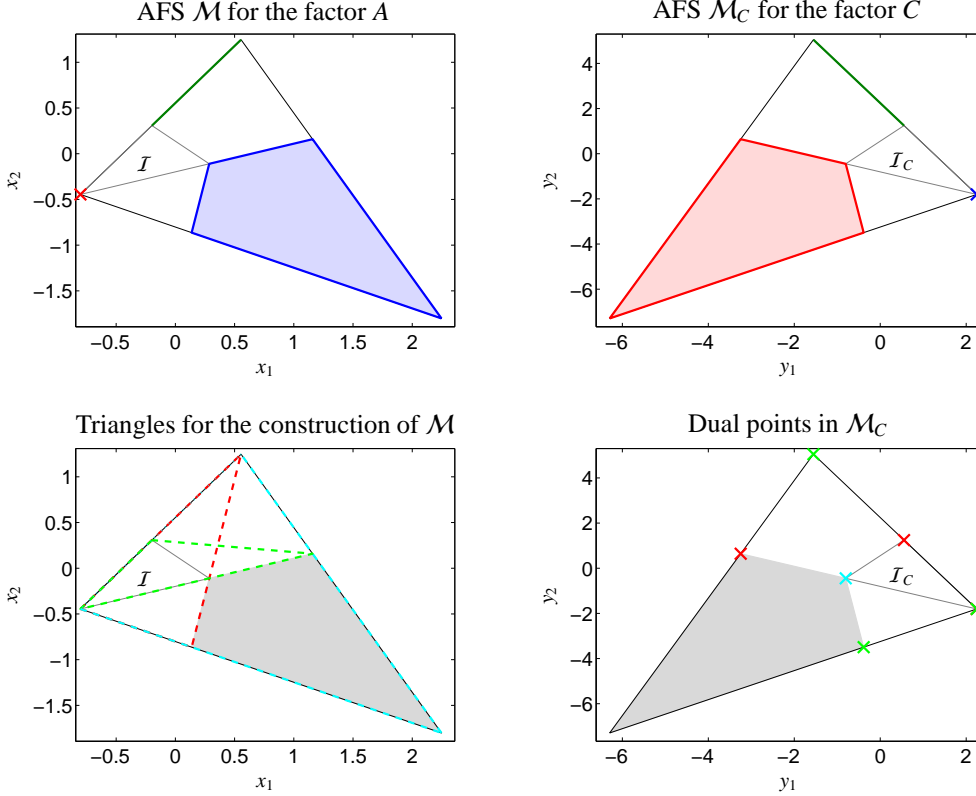


Figure 10: Construction of punctiform and line-shaped AFS segments by means of simultaneous Borgen plots. Upper row: The AFS sets \mathcal{M} and \mathcal{M}_C for the model problem from Sec. 4.4 with D by (15) consist each of a punctiform, a line-shaped and a 2D-area segment. Lower row: Triangles for the construction of \mathcal{M} which yield significant points for the construction of \mathcal{M}_C . Lower left: The red and the green triangles (broken lines) lead to the dot and the line segment as well as to two significant vertices of the two-dimensional AFS segment. The last significant point is related to the triangle I . The red and the green triangles yields the the dual points for \mathcal{M}_C (lower right) which define the dot and the line segment as well as to two significant points of the area segment. The last significant point (cyan) of \mathcal{M}_C is related to the cyan triangle (broken line) in \mathcal{M} . The black lines are the boundaries of \mathcal{F} and \mathcal{F}_C and the gray lines circumscribe I and I_C . The two-dimensional AFS segments are filled in gray.

concentration profiles are computed on the time interval $t \in [0, 30]$. We consider in this interval $k \in \{100, 250, 500, 1000, 2500\}$ equidistant grid points.

The continuous spectra are assumed to be

$$\begin{aligned}
 s_X(\lambda) &= \exp\left(-\frac{(\lambda-10)^2}{1000}\right) + \frac{1}{4} \exp\left(-\frac{(\lambda-75)^2}{10}\right), \\
 s_Y(\lambda) &= \exp\left(-\frac{(\lambda-20)^2}{1000}\right) + \frac{1}{4} \exp\left(-\frac{(\lambda-45)^2}{10}\right), \\
 s_Z(\lambda) &= \frac{19}{20} \exp\left(-\frac{(\lambda-30)^2}{1000}\right) + \frac{1}{4} \exp\left(-\frac{(\lambda-5)^2}{10}\right)
 \end{aligned}$$

for $\lambda \in [0, 100]$. We consider equidistant subdivisions of this interval with $n \in \{100, 200, 300, 500, 1000\}$ grid points. Thus the matrix elements of the spectral mixture data matrix D read

$$D_{ij} = c_X(t_i)s_X(\lambda_j) + c_Y(t_i)s_Y(\lambda_j) + c_Z(t_i)s_Z(\lambda_j)$$

for $i = 1, \dots, k$ and $j = 1, \dots, n$. Fig. 11 shows the true

factors, the mixed spectra, i.e. the rows of D , and the AFS sets \mathcal{M} and \mathcal{M}_C .

5.2. Polygon construction

The outer polygon \mathcal{F} and the inner polygon I are required for the geometric construction of the AFS \mathcal{M} . The \mathcal{F}_C and I_C are needed for \mathcal{M}_C . The inner polygons I resp. I_C are the convex hulls of the vectors a_i resp. b_i , see (6)–(9). In our program code we use the MATLAB routine `convhull`. Sec. 3.5 explains how these polygons lead to a fast algorithm to form the outer polygons \mathcal{F} and \mathcal{F}_C .

Table 1 lists the computation times for the new techniques to construct these four polygons and compares these with the timing data of the *Generalized Borgen plots* module and the polygon inflation method in its implementation in the *Complementarity & AFS* module of the *FACPACK* software. These computations we carried out for the model problem for five combinations

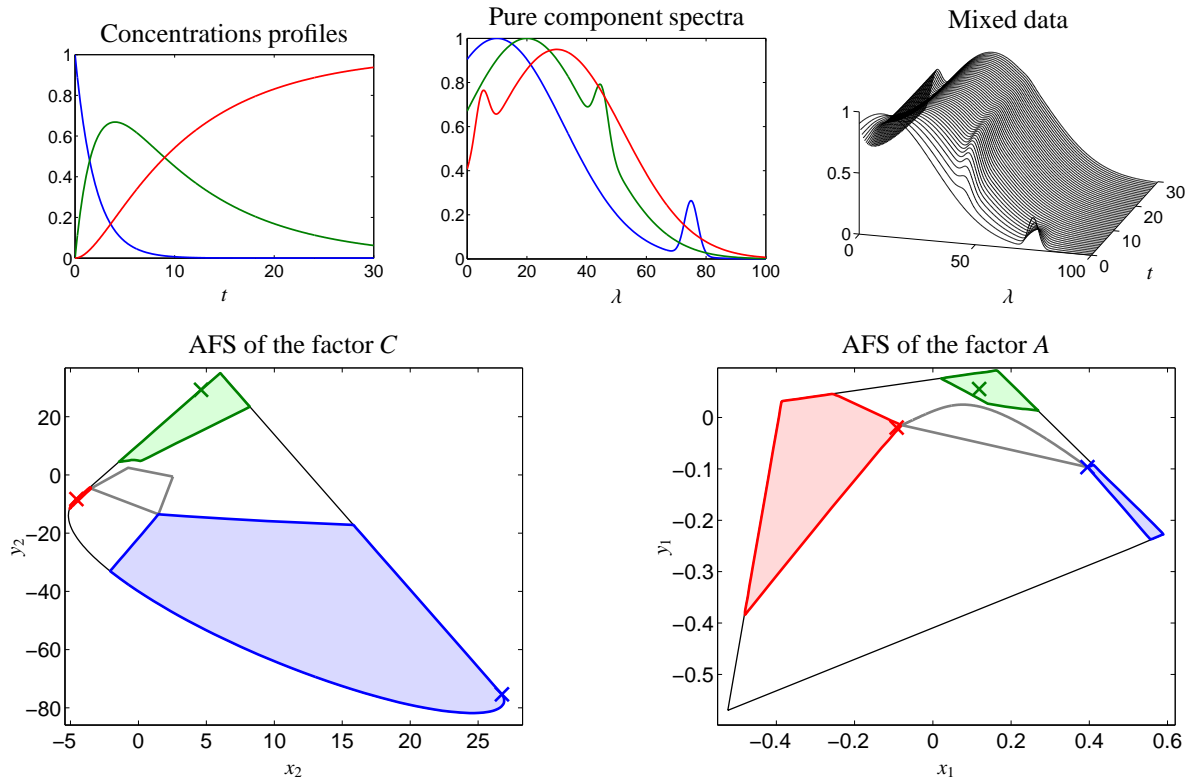


Figure 11: The model data as used in Sec. 5 with $k = 500$ spectra with each $n = 300$ spectral channels. Thus $D \in \mathbb{R}^{500 \times 300}$. Upper row: The concentration profiles of the three components (left), the associated pure component spectra (center) and the mixed spectra forming the rows of D (right, only every 10th spectrum is plotted). Lower row: The AFS set \mathcal{M}_C (left) and the AFS set \mathcal{M} (right). Both AFS sets consist of three isolated segments, which are plotted in the color blue, green and red. The true solutions are marked by crosses. The boundaries of the two FIRPOL-sets \mathcal{F}_C and \mathcal{F} are marked by black solid lines and the INNPOL-sets \mathcal{I}_C and \mathcal{I} by gray solid lines.

of the dimension variables k and n . The results clearly demonstrate the benefit of the new indirect approach to compute the dual pairs of polygons.

5.3. Simultaneous computation of the AFS sets

For the simultaneous construction of \mathcal{M} and \mathcal{M}_C we use a $k \times n$ discretization of the model problem with $k = 1000$ and $n = 500$. For these problem dimensions the polygon FIRPOL \mathcal{F} has 85 vertices and INNPOL \mathcal{I} has 1000 vertices and edges, which results in 1000 vertices of the dual polygon \mathcal{F}_C .

We use m_{equi} equiangular tangents of \mathcal{I} . Most of these tangents run only through vertices of \mathcal{I} and not through edges of \mathcal{I} . We additionally consider all tangents of edges of \mathcal{I} . Finally, we add those tangents of \mathcal{I} which run through the vertices of \mathcal{F} , see also Sec. 4.2.

Table 2 lists the numbers of equiangular tangents and the total numbers of tangents m_{all} together with the computation times. The simultaneous construction saves about 30% of the computation time compared to the separate and independent constructions of \mathcal{M} and \mathcal{M}_C .

Remark 5.1. As explained in Sec. 4.3 the boundary of \mathcal{M}_C has a doubled spatial resolution. For this reason, we have doubled the number of tangents for the separate and independent computation of \mathcal{M}_C for all the computations which underlie the timing data listed in Table 2.

5.4. Comparison to other algorithms

Finally, we compare the implementation of simultaneous Borgen plots to the efficient *FACPACK* implementations [29, 25] of the polygon inflation method [27, 28] and to the generalized Borgen plots method [11, 12]. Again, the model problem is used with varying dimensions k and n . Polygon inflation is used with the control parameters $\varepsilon_b = \delta = 10^{-3}$. For the generalized Borgen plots the control parameter is $\alpha_{\text{rot}} = 0.1$. The simultaneous Borgen plot algorithm is started with $m_{\text{equi}} = 5000$ equiangular tangents. This corresponds to an incremental rotation angle $\alpha_{\text{rot}} = 360/5000 = 0.072$ in degrees.

The computation times are listed in Table 3. Again, the simultaneous Borgen plot algorithm is clearly the fastest. Compared to the polygon inflation method it saves sometimes more than 90% of the computation time. A similar outcome can be stated for the generalized Borgen plots. The substantial acceleration of the new method is based not only on the effectiveness of the new algorithm but also on its efficient computer implementation (which is trimmed to maximal speed but is still not optimized to display punctiform and line-shaped AFS segments). These findings should not diminish the value of the polygon inflation method and the generalized Borgen plots algorithm in their *FAC-PACK* implementations. The latter very stable implementations are by orders of magnitudes faster than, e.g., the elementary grid search approach for approximating the AFS.

6. Conclusion and outlook

The geometric construction of Borgen plots is sometimes considered to be the most reliable, first-principle approach to analyze the rotational ambiguity of model-free MCR factorizations. The new fast and simultaneous construction of the AFS for the two factors C and S on the basis of the duality/complementarity theory can support any MCR studies. A drawback of Borgen plots and of simultaneous Borgen plots is that they can only be applied to noise-free and non-perturbed spectral data. This restricts these approaches to model data. Another drawback of the geometric constructions is that no approach has yet been devised for a combination with soft constraints as unimodality or monotonicity; see [3, 32, 20] for such combinations in the context of numerical optimization-based MCR methods. Equality constraints, see [4, 3, 30], can principally be integrated to the Borgen plot techniques.

In the forthcoming second part to this paper we intend to present a hybrid technique which combines simultaneous Borgen plots with the polygon inflation method. The resulting method is universal and as robust with respect to noise and perturbations as are the polygon inflation, the triangle enclosure technique [7] and the grid-search method [34, 2]. The hybrid and simultaneous construction method is still faster than the classical Borgen plots. This hybrid method combines the advantages of the numerical, optimization-based techniques with the geometric AFS constructions.

References

- [1] H. Abdollahi, M. Maeder, and R. Tauler. Calculation and Meaning of Feasible Band Boundaries in Multivariate Curve Resolution of a Two-Component System. *Anal. Chem.*, 81(6):2115–2122, 2009.
- [2] H. Abdollahi and R. Tauler. Uniqueness and rotation ambiguities in Multivariate Curve Resolution methods. *Chemom. Intell. Lab. Syst.*, 108(2):100–111, 2011.
- [3] S. Beyramysoltan, H. Abdollahi, and R. Rajkó. Newer developments on self-modeling curve resolution implementing equality and unimodality constraints. *Anal. Chim. Acta*, 827(0):1–14, 2014.
- [4] S. Beyramysoltan, R. Rajkó, and H. Abdollahi. Investigation of the equality constraint effect on the reduction of the rotational ambiguity in three-component system using a novel grid search method. *Anal. Chim. Acta*, 791(0):25–35, 2013.
- [5] O.S. Borgen and B.R. Kowalski. An extension of the multivariate component-resolution method to three components. *Anal. Chim. Acta*, 174:1–26, 1985.
- [6] A. Golshan, H. Abdollahi, S. Beyramysoltan, M. Maeder, K. Neymeyr, R. Rajkó, M. Sawall, and R. Tauler. A review of recent methods for the determination of ranges of feasible solutions resulting from soft modelling analyses of multivariate data. *Anal. Chim. Acta*, 911:1–13, 2016.
- [7] A. Golshan, H. Abdollahi, and M. Maeder. Resolution of Rotational Ambiguity for Three-Component Systems. *Anal. Chem.*, 83(3):836–841, 2011.
- [8] A. Golshan, M. Maeder, and H. Abdollahi. Determination and visualization of rotational ambiguity in four-component systems. *Anal. Chim. Acta*, 796(0):20–26, 2013.
- [9] G.H. Golub and C.F. Van Loan. *Matrix Computations*. Johns Hopkins Studies in the Mathematical Sciences. Johns Hopkins University Press, Baltimore, MD, 2012.
- [10] R.C. Henry. Duality in multivariate receptor models. *Chemom. Intell. Lab. Syst.*, 77(1-2):59–63, 2005.
- [11] A. Jürß, M. Sawall, and K. Neymeyr. On generalized Borgen plots. I: From convex to affine combinations and applications to spectral data. *J. Chemom.*, 29(7):420–433, 2015.
- [12] A. Jürß, M. Sawall, and K. Neymeyr. On generalized Borgen plots. II: The line-moving algorithm and its numerical implementation. *J. Chemom.*, 30:636–650, 2016.
- [13] W.H. Lawton and E.A. Sylvestre. Self modelling curve resolution. *Technometrics*, 13:617–633, 1971.
- [14] M. Maeder and Y.M. Neuhold. *Practical data analysis in chemistry*. Elsevier, Amsterdam, 2007.
- [15] E. Malinowski. *Factor analysis in chemistry*. Wiley, New York, 2002.
- [16] A. Meister. Estimation of component spectra by the principal components method. *Anal. Chim. Acta*, 161:149–161, 1984.
- [17] H. Minc. *Nonnegative matrices*. John Wiley & Sons, New York, 1988.
- [18] K. Neymeyr and M. Sawall. On an SVD-free approach to the complementarity and coupling theory: A note on the elimination of unknowns in sums of dyadic products. *J. Chemom.*, 30:30–36, 2016.
- [19] K. Neymeyr, M. Sawall, and D. Hess. Pure component spectral recovery and constrained matrix factorizations: Concepts and applications. *J. Chemom.*, 24:67–74, 2010.
- [20] N. Rahimdoust, M. Sawall, K. Neymeyr, and H. Abdollahi. Investigating the effect of flexible constraints on the accuracy of self-modeling curve resolution methods in the presence of perturbations. *J. Chemom.*, 30(5):252–267, 2016.
- [21] R. Rajkó. Natural duality in minimal constrained self modeling curve resolution. *J. Chemom.*, 20(3-4):164–169, 2006.

- [22] R. Rajkó. Additional knowledge for determining and interpreting feasible band boundaries in self-modeling/multivariate curve resolution of two-component systems. *Anal. Chim. Acta*, 661(2):129–132, 2010.
- [23] R. Rajkó and K. István. Analytical solution for determining feasible regions of self-modeling curve resolution (SMCR) method based on computational geometry. *J. Chemom.*, 19(8):448–463, 2005.
- [24] M. Sawall, C. Fischer, D. Heller, and K. Neymeyr. Reduction of the rotational ambiguity of curve resolution techniques under partial knowledge of the factors. Complementarity and coupling theorems. *J. Chemom.*, 26:526–537, 2012.
- [25] M. Sawall, A. Jürß, and K. Neymeyr. FACPACK: A software for the computation of multi-component factorizations and the area of feasible solutions, Revision 1.3. FACPACK homepage: <http://www.math.uni-rostock.de/facpack/>, 2015.
- [26] M. Sawall, A. Jürß, H. Schröder, and K. Neymeyr. *On the analysis and computation of the area of feasible solutions for two-, three- and four-component systems*, volume 30 of Data Handling in Science and Technology, “Resolving Spectral Mixtures”, Ed. C. Ruckebusch, chapter 5, pages 135–184. Elsevier, Cambridge, 2016.
- [27] M. Sawall, C. Kubis, D. Selent, A. Börner, and K. Neymeyr. A fast polygon inflation algorithm to compute the area of feasible solutions for three-component systems. I: Concepts and applications. *J. Chemom.*, 27:106–116, 2013.
- [28] M. Sawall and K. Neymeyr. A fast polygon inflation algorithm to compute the area of feasible solutions for three-component systems. II: Theoretical foundation, inverse polygon inflation, and FAC-PACK implementation. *J. Chemom.*, 28:633–644, 2014.
- [29] M. Sawall and K. Neymeyr. *How to compute the Area of Feasible Solutions, A practical study and users’ guide to FAC-PACK*, volume in Current Applications of Chemometrics, ed. by M. Khanmohammadi, chapter 6, pages 97–134. Nova Science Publishers, New York, 2014.
- [30] M. Sawall and K. Neymeyr. On the area of feasible solutions and its reduction by the complementarity theorem. *Anal. Chim. Acta*, 828:17–26, 2014.
- [31] M. Sawall and K. Neymeyr. A ray casting method for the computation of the area of feasible solutions for multicomponent systems: Theory, applications and FACPACK-implementation. *Anal. Chim. Acta*, 960:40–52, 2017.
- [32] M. Sawall, N. Rahimdoust, C. Kubis, H. Schröder, D. Selent, D. Hess, H. Abdollahi, R. Franke, Börner A., and K. Neymeyr. Soft constraints for reducing the intrinsic rotational ambiguity of the area of feasible solutions. *Chemom. Intell. Lab. Syst.*, 149, Part A:140–150, 2015.
- [33] G.W. Stewart. On the early history of the singular value decomposition. *SIAM Review*, 35:551–556, 1993.
- [34] M. Vosough, C. Mason, R. Tauler, M. Jalali-Heravi, and M. Maeder. On rotational ambiguity in model-free analyses of multivariate data. *J. Chemom.*, 20(6-7):302–310, 2006.
- [35] E. Widjaja, C. Li, W. Chew, and M. Garland. Band target entropy minimization. A robust algorithm for pure component spectral recovery. Application to complex randomized mixtures of six components. *Anal. Chem.*, 75:4499–4507, 2003.

dimensions		computation times [10^{-3} s]					
k	n	direct computation (GBP)		approx. (PIA)		indirect computation (new)	
		$\mathcal{F} \& \mathcal{I}$	$\mathcal{F}_C \& \mathcal{I}_C$	\mathcal{F}	\mathcal{F}_C	$\mathcal{I} \& \mathcal{I}_C$	$\mathcal{F} \& \mathcal{F}_C$
100	100	194	481	6.89	42.08	0.17	0.11
250	200	500	2 794	9.82	69.43	0.22	0.21
500	300	1 014	11 284	12.37	99.42	0.32	0.43
1000	500	2 655	45 252	16.38	81.51	0.50	0.85
2500	1000	10 176	-	28.11	212.86	1.09	2.80

Table 1: Computation times for \mathcal{F} , \mathcal{F}_C , \mathcal{I} and \mathcal{I}_C for various dimensions of D . These sets are the basis for the geometric constructions of \mathcal{M} and \mathcal{M}_C . First approach: Direct and separate computation of each of these four sets by means of the *Generalized Borgen plots* (GBP) module of *FACPACK*. Second approach: Approximation of \mathcal{F} and \mathcal{F}_C by the polygon inflation method (PIA) with the control parameters $\varepsilon_b = \delta = 10^{-4}$ by using the software implementation in the *Complementarity & AFS* module of *FACPACK*. Third approach: Direct computations of \mathcal{I} and \mathcal{I}_C and indirect computation of \mathcal{F} and \mathcal{F}_C by using the duality theory of Sec. 3.5 based on Thm. 3.6 and Cor. 3.7. The indirect computation of \mathcal{F} and \mathcal{F}_C is clearly the fastest approach.

# tangents		computation times [s]			
m_{equi}	m_{all}	separate comp.			simult. comp.
		\mathcal{M}	\mathcal{M}_C	$\mathcal{M} \& \mathcal{M}_C$	$\mathcal{M} \& \mathcal{M}_C$
100	1105	0.492	0.039	0.531	0.497
1000	1966	0.541	0.069	0.610	0.554
2500	3400	0.624	0.127	0.751	0.653
5000	5791	0.771	0.240	1.011	0.835
10000	10572	1.088	0.522	1.610	1.257
15000	15353	1.437	0.886	2.323	1.765

Table 2: The computation times for the two AFS sets \mathcal{M} and \mathcal{M}_C by the classical geometric construction (Borgen plots) and the simultaneous Borgen plots. The dimensions of the model data matrix D are $k = 1000$ and $n = 500$. The number of equiangular tangents m_{equi} varies between 100 and 15000. Additional tangents are added at critical boundary points, see Sec. 4.2. The computation times are listed for the separate and independent computation of \mathcal{M} and \mathcal{M}_C and also for the simultaneous algorithm. According to Remark 5.1 the set \mathcal{M}_C has about a doubled spatial resolution.

dimensions		computation times [s]						
k	n	PIA			GBP			SBP
		\mathcal{M}	\mathcal{M}_C	$\mathcal{M} \& \mathcal{M}_C$	\mathcal{M}	\mathcal{M}_C	$\mathcal{M} \& \mathcal{M}_C$	$\mathcal{M} \& \mathcal{M}_C$
100	100	1.56	2.05	3.61	0.91	1.14	2.05	0.090
250	200	3.15	4.35	7.50	1.39	3.59	4.98	0.149
500	300	5.52	7.67	13.19	2.29	12.29	14.58	0.289
1000	500	10.93	13.17	24.10	4.82	46.67	51.49	0.835
2500	1000	23.36	26.08	49.44	16.46	-	-	6.254

Table 3: Comparison of simultaneous Borgen plots (SBP) to the polygon inflation algorithm (PIA) and the generalized Borgen plots method (GBP). The *FACPACK* implementations of PIA and GBP were used. The computation of \mathcal{M}_C by GBP was canceled manually after 3 minutes of computation without a result.